Winter-to-Spring Transition in East Asia: A Planetary-Scale Perspective of the South China Spring Rain Onset

L. H. LINHO

Department of Atmospheric Sciences, National Taiwan University, Taipei, Taiwan

XIANGLEI HUANG*

Program in Atmospheric and Oceanic Sciences, Princeton University, Princeton, New Jersey

NGAR-CHEUNG LAU

NOAA/Geophysical Fluid Dynamics Laboratory, Princeton University, Princeton, New Jersey

ABSTRACT

Analysis of observations from 1979 to 2002 shows that the seasonal transition from winter to spring in East Asia is marked with a distinctive event—the onset of the south China spring rain (SCSR). In late February, the reduced thermal contrast between ocean and land leads to weakening of the Asian winter monsoon as well as the Siberian high and the Aleutian low. Meanwhile, convection over Australia and the western Pacific Maritime Continent is suppressed on the passage of the dry phase of a Madden–Julian oscillation (MJO). In conjunction with the seasonal march of monsoon circulation in the Indonesian–Australian sector, this MJO passage weakens the local thermally direct cell in the East Asia–Australia sector. This development is further accompanied by a series of adjustments in both the tropics and mid-latitudes. These changes include attenuation of the planetary stationary wave, considerable weakening of the westerly jet stream over much of the central Pacific adjacent to Japan, and reduction of baroclinicity near the East Asian trough. The influence of concurrent local processes in midlatitudes on the SCSR onset is also important. The weakened jet stream is associated with confinement of frontal activities to the coastal regions of East Asia as well as with rapid expansion of the subtropical Pacific high from the eastern Pacific to the western Pacific. A parallel analysis using output from an experiment with a GFDL-coupled GCM shows that the above sequence of circulation changes is well simulated in that model.

1. Introduction

The East Asian sector (110°–130°E) is very sensitive to seasonal transition—not only because it is situated between the largest ocean and the largest continent, but also because the atmospheric circulation over this region is strongly influenced by a Hadley circulation linking the two hemispheres. Therefore, it is not surprising that the observed time–latitude distribution of the climatologically averaged rain rate in this area exhibits almost all essential features of the Asian–Pacific summer monsoon (LinHo and Wang 2002). What distinguishes the East Asian rainfall regime from other monsoon regimes is its stepwise evolution within the rainy season. The annual cycle is clearly separated into a dry phase and a wet phase (rainy season). The rainy season can be further subdivided into five "natural" subseasons: the south China spring rain (SCSR), the pre-mei-yu period, the grand onset period, the monsoon gyre period, and the autumn trough period. The development from the pre-mei-yu period to the autumn trough period has been extensively documented and studied by many investigators (e.g., Cheang 1986; Ueda et al. 1995; Wu and Wang 2001; LinHo and Wang 2002; Wang et al. 2004; and references therein). However,

* Current affiliation: Department of Atmospheric, Oceanic, and Space Sciences, University of Michigan, Ann Arbor, Michigan.

Corresponding author address: Xianglei Huang, Department of Atmospheric, Oceanic, and Space Sciences, University of Michigan, 2455 Hayward St., Ann Arbor, MI 48109-2143.
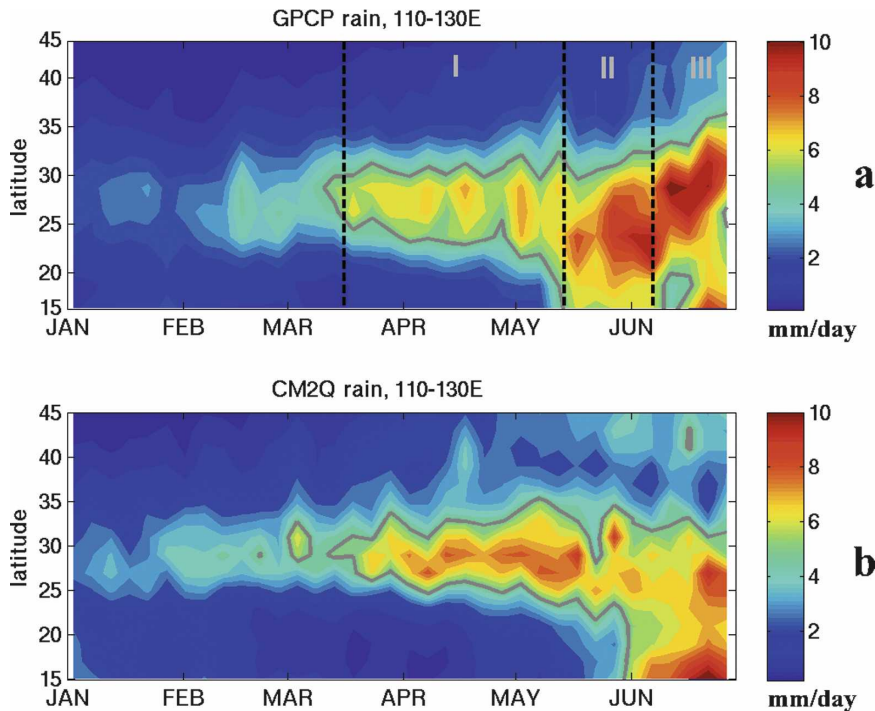E-mail: xianglei@umich.edu

FIG. 1. (a) Time–latitude distribution of the observed climatological rainfall rate (mm day^{-1}) over 110°–130°E based on 1979–2002 GPCP data at pentad resolution. "Natural" subseasons of rainy season are indicated: (I) the SCSR, (II) the pre-mei-yu period, and (III) the grand onset period. The boldface purple contour line corresponds to a rainfall rate of 5 mm day^{-1}. (b) The corresponding distribution based on 20-yr output from the CM2Q control run.

based on the accessible literature, we found that the earliest part of the rainy season in East Asia, the SCSR, has not been studied in comparable depth and breadth as other phases of the rainy season. In a synoptic-meteorology textbook widely used in China (Zhu et al. 1981), the major synoptic processes related to the persistent spring rain over central China and south China were briefly described. Tian and Yasunari (1998) examined the climatological aspects of the SCSR and proposed a mechanism for this persistent spring rain event, emphasizing the role played by the low-level southwesterly jet. Figure 1a shows that the SCSR starts near mid-March, two months before the onset of the pre-mei-yu period. The SCSR occurs within the 25°–30°N zone, and, in many ways, has features similar to the well-known mei-yu (plum rain) period, with strong southwesterly winds near the coastal region, and fronts approaching the South and East China Seas. Many meso-scale convective systems are triggered by topography such as Nan Ling (South Hill, 25°–30°N, 110°–120°E, with an average height of 1200 m) and the Central Mountain Range of Taiwan (average height of 2500 m). Occasionally, the frontal movements become slow or even stagnant, thus leading to persistent rain for several

days, in analogy with the synoptic situation associated with a mei-yu front. Near the mountainous border between Guangdong and Fujian provinces of southern China, the rain in March and April could account for one-quarter to one-third of the annual total precipitation. Because the SCSR is the first persistent rainfall after the dry winter season, its timing and intensity directly affect regional agricultural and economic activities. This phenomenon is therefore of great concern to the densely populated communities in south China (Chen et al. 2003).

The onset of the SCSR is not an isolated event, but is part of a family of phenomena that are closely associated with the transition of the global circulation from boreal winter to spring within a relatively short duration. Extratropical processes, such as the revival of the Pacific storm-track activity after its midwinter suppression can directly influence the jet stream and the precipitation in south China during the winter-to-spring transition (Nakamura 1992). A recent study by Wan and Wu (2007) established the influence of the Tibetan Plateau on the SCSR. In addition to these processes, it is also worthwhile to investigate the possible influence of tropical activities on the SCSR onset. The primary

purpose of this study is to offer a description of the myriad meteorological changes accompanying the SCSR onset, and the interrelationships between such changes, with emphases on the planetary perspective of this phenomenon and its linkage with tropical phenomena. Our analyses of these features are conducted using observational datasets, as well as output from a simulation based on a contemporary general circulation model (GCM). The appearance of the phenomena of interest in both observed and modeled atmospheres would enhance our confidence in the robustness of these signals. The joint observational and model diagnoses of the processes related to SCSR also provide valuable insights on the fidelity of the GCM in reproducing essential characteristics of one of the most prominent monsoon systems in the observed atmosphere.

The presentation of our findings is organized as follows. Section 2 describes the observational datasets and the global coupled climate model examined in this study. A climatological picture of the seasonal transition from boreal winter to spring in East Asia is presented in section 3. The interplay among the Asian winter monsoon, the Hadley circulation in the local meridional plane, and Madden–Julian oscillation (MJO), and the roles of these features in the SCSR phenomenon, are discussed in section 4. Composite maps of various atmospheric fields before and after the SCSR onset are shown in section 5. Conclusions and discussions on the seasonality of East Asian climate are given in section 6.

2. Data and model description

Most of our analysis is applied to data with a temporal resolution of 5 days (a pentad). The 5-day averaging procedure is effective in suppressing synoptic disturbances, and yet retains the prominent features on the time scales of interest. The observed precipitation field is based on pentad-resolution data from the Global Precipitation Climatology Project (GPCP; Xie et al. 2003). Observations of other fields are based on the National Centers for Environmental Prediction–National Center for Atmospheric Research (NCEP–NCAR) reanalyses (Kalnay et al. 1996). For both datasets, the climatology is computed by averaging the data for 1979–2002.

Model diagnosis is performed on the output from a multiple-century control run of the Geophysical Fluid Dynamics Laboratory Climate Model, version 2.0 (GFDL CM2.0), a global coupled climate model (Delworth et al. 2006). We shall henceforth refer to this experiment as CM2Q. The spatial resolution of the land and atmospheric components in the CM2.0 is 2° latitude × 2.5° longitude. The atmospheric component has

24 vertical levels. The resolution of the ocean component is 1° in latitude and longitude outside of the tropics. The meridional resolution equatorward of 30° latitude increases gradually to 1/3° at the equator. Flux adjustments are not employed in this model. The CM2Q experiment yields a stable and realistic climate (see Delworth et al. 2006). To compare with observations in sections 3–4, the model output from a comparable period of 20 yr (corresponding to model years 101–120), is used to construct the model climatology. In section 5, the output for a longer, 100-yr period (model years 101–200) is analyzed to delineate circulation changes relative to the SCSR onset.

Figure 1b shows the time–latitude distribution of the climatological precipitation over East Asia as simulated in CM2Q (averages of model years 101–120). Compared to the observation (Fig. 1a), the model generates much more precipitation in the 15°–20°N zone in June, and the northward progression of the onset of the monsoon from 20° to 40°N during June is not well simulated.[1] However, the climatological onset of the SCSR in the model is largely consistent with the observation with regards to timing, latitudinal position, and precipitation amount. As can be inferred from Fig. 1a, the time derivatives of the observed climatological precipitation over south China (23°–30°N, not shown here) indicate that precipitation starts to increase in pentad 14 (centered on 9 March), with maximum rate of increase being attained in pentad 15. The rate of increase in pentad 15 is about twice that in pentads 14 and 16. Similarly, the rate of increase of CM2Q climatological precipitation (Fig. 1b) reaches a maximum in pentad 16, and is more than twice that in pentads 15 and 17. This favorable comparison between model and observations encourages us to conduct a parallel analysis of the SCSR onset using both observations and CM2Q output.

Figure 2 shows the time–latitude distributions of CM2Q-simulated precipitation over the East Asian sector, as averaged over four other consecutive 20-yr segments within the period spanning from model years 121 to 200. It can be seen that CM2Q does exhibit decadal variability. Yet, as far as the climatology to be discussed in later sections is concerned, we find that the influence of decadal variability on such climatological estimates is limited and we reach essentially the same conclusions if we analyze output of the other 20-yr periods.

---

[1] The simulation of the poleward advance of rain belts in the June–July period is much improved in recent experiments with a higher-resolution (0.5° latitude × 0.625° longitude) finite-volume version of the atmospheric component of the GFDL climate model.
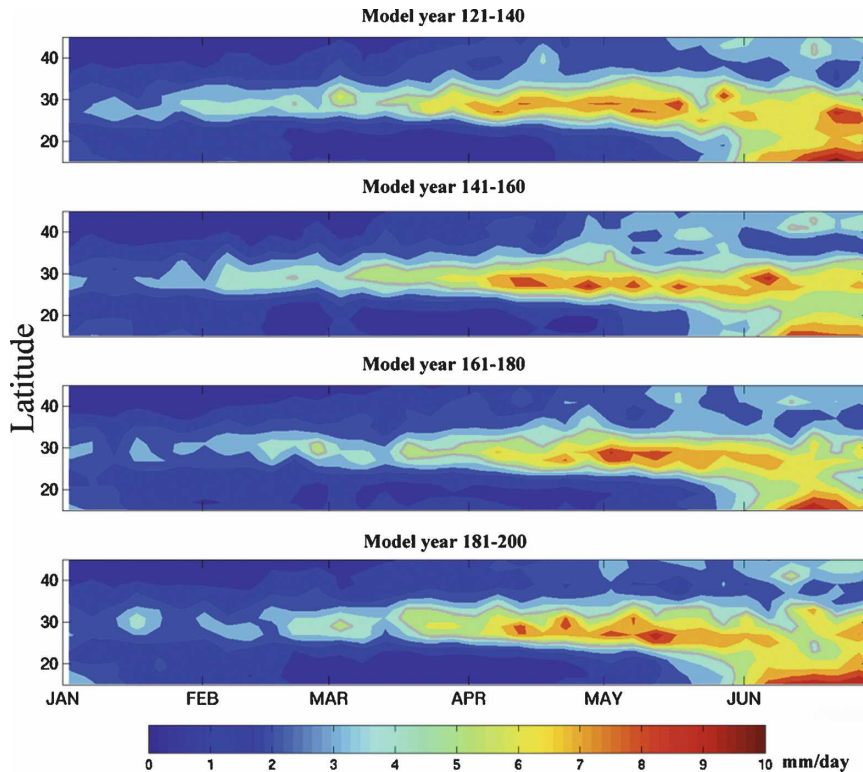
FIG. 2. Same as Fig. 1b, except that different 20-yr segments of model output are used. Four segments (corresponding to model years 121–140, 141–160, 161–180, and 181–200, respectively) are plotted here. The boldface gray contour lines correspond to 5 mm day^{-1} rainfall rate.

3. Winter-to-spring transition of the Asian monsoon

The climatological springtime rain belt, as shown in Fig. 1, begins in about mid-March (i.e., pentad 15, or 12–16 March). Therefore, we illustrate the transition from boreal winter to spring by contrasting the nine-pentad averages of climatological sea level pressure (SLP), precipitation, and 200-hPa wind before and after pentad 15. Figure 3a shows the observed climatology for averages over pentads 6–14 (26 January–11 March). The Asian continent is under influence of the Siberian high, which extends southeastward over eastern China. Also evident in Fig. 3a is the jet stream in the East Asia–western Pacific sector (see arrows), which attains maximum intensity over the region east of southern Japan. The strong temperature gradients in the vicinity of this jet stream (not shown) are conducive to frequent formation of extratropical cyclones. The ensuing eastward migration and growth of these baroclinic disturbances result in an elongated zone of strengthened synoptic-scale activity stretching all the way across the Pacific basin at 40°–45°N. This region of vigorous eddy activity, often referred to as the midlatitude "storm track" (e.g., Blackmon et al. 1977), is characterized by

enhanced precipitation, as illustrated by shading in Fig. 3a. During the period of pentads 6–14, the subtropical Pacific high is confined largely to the southeastern edge of the North Pacific basin.

The aforementioned East Asian jet stream is maintained by a local, thermally direct circulation (Blackmon et al. 1977; Lau and Li 1984). The extensive convective systems over Australia and Indonesia induce northward, cross-equatorial divergent winds at the upper troposphere, which in turn lead to eastward accelerations of the upper-level jet. Near the surface, strong northeasterly winds blow across the equator over the Indian Ocean (as part of the Indian winter monsoon) and the western Pacific (as part of the trade wind system). These cross-equatorial flows then converge with the southeasterly trade winds in the Southern Hemisphere, thus sustaining strong convection in the Indonesian–Australian summer monsoon region. Hence, the East Asian winter monsoon and the Indonesian–Australian summer monsoon act in concert to maintain the thermally direct circulation during the December–February period.

The observed climatological averages over pentads 16–24 (17 March–30 April) are shown in Fig. 3b. The following are the major differences from the patterns
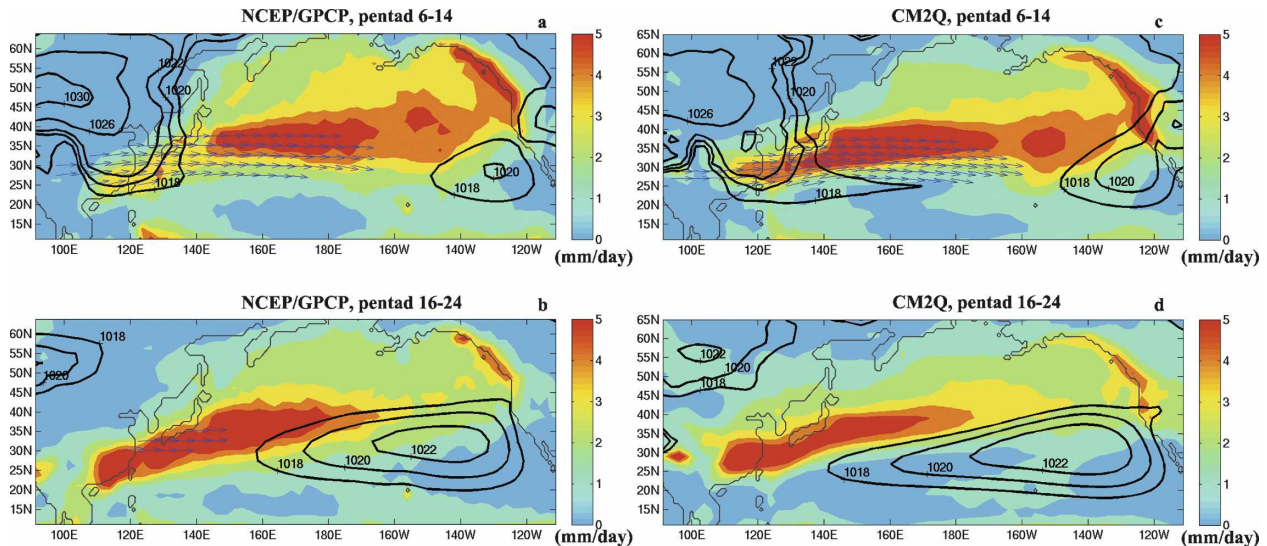
FIG. 3. (a) Observed climatological average over pentads 6–14 (26 Jan–11 Mar) based on NCEP and GPCP data for the 1979–2002 period. Precipitation (mm day^{-1}) is represented by color shading. SLP (hPa) is indicated by contours. Only contours around high pressure centers are drawn. Wind vectors at 200 hPa with speed greater than 50 m s^{-1} are depicted by arrows. (b) Same as (a), except that the averages are performed over pentads 16–24 (17 Mar–30 Apr). (c), (d) Model counterparts of (a), (b) based on a 20-yr simulation of the CM2Q control run.

for pentads 6–14 (Fig. 3a): 1) the Siberian high retreats toward the Lake Baikal region (near 53°N, 108°E), 2) the upper-level jet stream is discernible only in a spatially limited site near Japan, 3) the precipitation intensity is much enhanced in a belt extending northeastward from southeastern China to the western Pacific, whereas the rain rate along the eastern portion of the North Pacific storm track is considerably reduced, and 4) the subtropical Pacific high expands noticeably toward the central and western Pacific. This phase of the seasonal cycle is characterized by weakening of the East Asian jet stream. Reduction of the intensity and longitudinal extent of the jet stream leads to decreased transient eddy activity and precipitation over the eastern portion of the extratropical Pacific. This development is, in turn, accompanied by rapid expansion of the subtropical Pacific anticyclone, the influence of which is felt as far west as the Indochina Peninsula by the end of the spring season (e.g., Ding 2004).

The model counterparts of Figs. 3a,b are shown in Figs. 3c,d, respectively. As mentioned in section 2, the model climatology is obtained using model output for a 20-yr duration. The diminution of the East Asian jet stream, the retreat of the Siberia high, and the expansion of the subtropical Pacific high from pentads 6–14 to 16–24 are all well captured in the CM2Q experiment. The GCM successfully simulates both the spatial characteristics and the amplitudes of these transitions from boreal winter to spring. The model, however, generates too much precipitation over southeastern China and

the adjoining ocean areas in pentads 6–14 (see Figs. 3a,c). Regardless, the model does show notable increases in the rain rate over southern China from pentads 6–14 to 16–24, in accordance with the observations.

4. Linking the seasonal transition to intraseasonal oscillations in the tropics and the strength of the local Hadley cell

As mentioned in the previous section, a local Hadley cell plays a critical role in sustaining the wintertime East Asian jet stream. We proceed to examine the evolution of this meridional circulation in late winter and early spring, and the manner in which this seasonal transition is modulated by a ubiquitous mode of variability in the tropics—the MJO (Madden and Julian 1971). We shall first take a close look at the evolution in 1986, and then extend the discussion to climatological averages.

a. The 1986 case

The slowdown of the local Hadley circulation in the East Asian sector can be studied in more detail by examining several variables closely related to this phenomenon. Figure 4 shows the latitude–time distributions of these fields averaged over 110°–130°E, as observed in the January–June period of 1986. In Fig. 4d, the negative extremum in the difference between the near-equatorial zonal winds at 200 and 850 hPa in
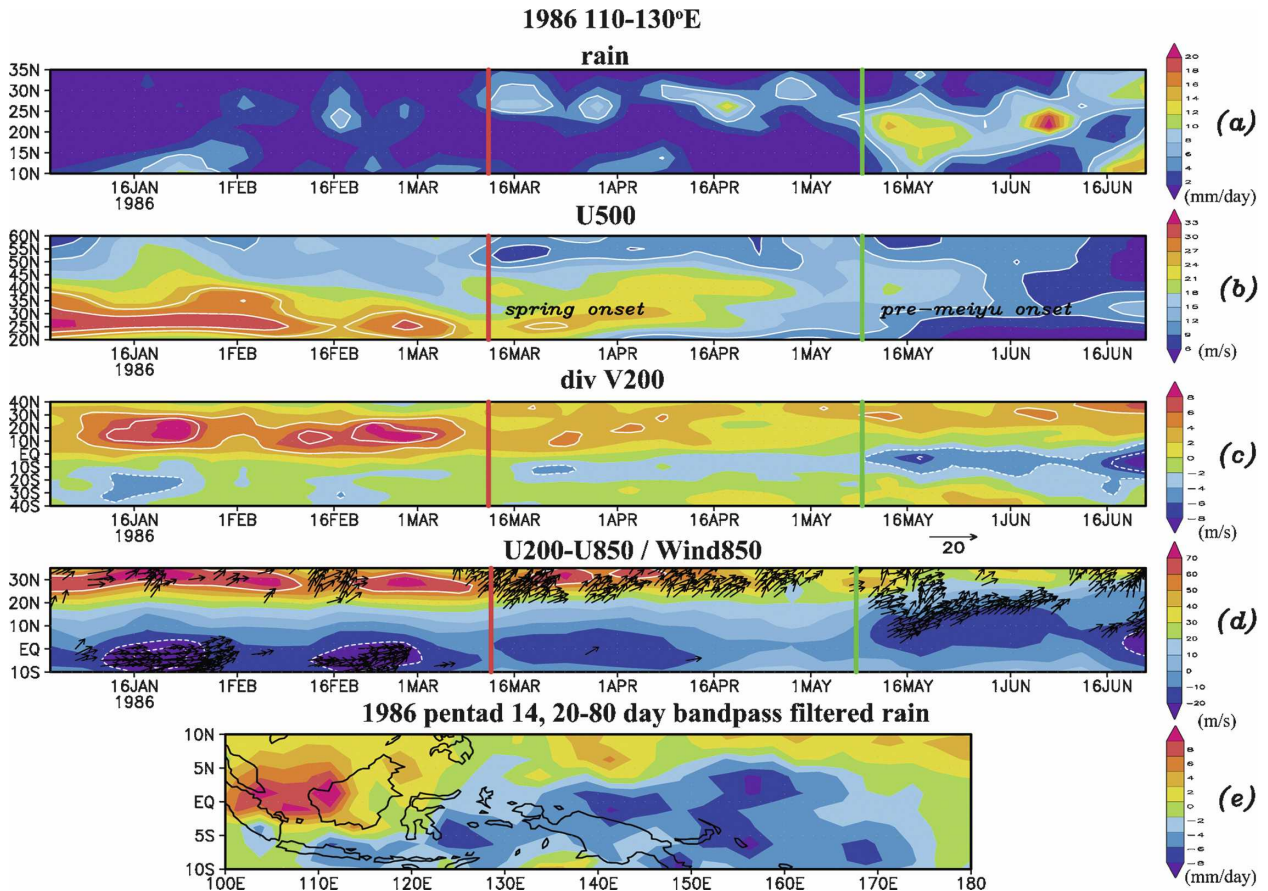
FIG. 4. (a)–(d) Time–latitude distributions averaged over the East Asia sector (110°–130°E) in 1986. (a) GPCP precipitation (white contour line corresponds to 5 mm day^{-1}); (b) the 500-hPa zonal wind; (c) the 200-hPa meridional divergent wind (warm colors indicate positive values and cold colors negative values); and (d) the difference between zonal wind at 200 and 850 hPa (baroclinity; warm colors indicate positive values and cold colors negative values). The arrows indicate the wind vectors at 850 hPa with a speed of more than 6 m s^{-1}. The scale for these vectors is plotted below. (e) The 20–80-day bandpass-filtered GPCP precipitation anomalies for pentad 14 in 1986. The red boldface lines in (a)–(e) indicate the onset of the SCSR, and the green boldface lines indicate the onset of the pre-mei-yu period.

mid-February is indicative of prevalent low-level westerlies and upper-level easterlies in this sector. The low-level westerly wind burst (see arrows near the equator in Fig. 4d) is associated with the passing of the wet phase of a MJO over the Indonesian–Australian sector.[2] As a result of this passage, there are surges of upper-level divergent winds toward the northern subtropics, as indicated in Fig. 4c. These surges of divergent winds then strengthen the upper-level jet, as can be seen from Fig. 4b. Meanwhile, no significant precipitation is observed between 24° and 35°N in this period

[2] Figures 4c,d indicate that in the first two months of 1986, the wet phase of the MJO passed over the Australian–Indonesian sector twice, once in mid-January and the other in mid-February. Both passages were also identified in another study of the MJO events in the 1985/86 winter season (Hsu et al. 1990).

(Fig. 4a). The 20–80-day bandpass-filtered precipitation data in Fig. 4e indicates that, in early to mid-March, the dry phase of the MJO passed over the Indonesian–Australian sector in the Southern Hemisphere. With such a passage, the magnitudes of both the vertical wind shear in the deep tropics and the upper-tropospheric divergent wind in the northern subtropics start to decrease, thus setting the stage for the attenuation of the local Hadley cell and the East Asian jet stream. Figure 4b shows that a secondary jet axis emerges near 40°N in mid-March but is not persistent. After mid-March, the strength of the primary jet is noticeably weaker than that observed in midwinter, and the jet axis starts to drift northward, reaching 45°N in early and mid-April.

A comparison between the Figs 5a,b and Figs 5c,d reveals a low-level cyclonic tendency near pentad 14 over southern China and the nearby maritime regions,
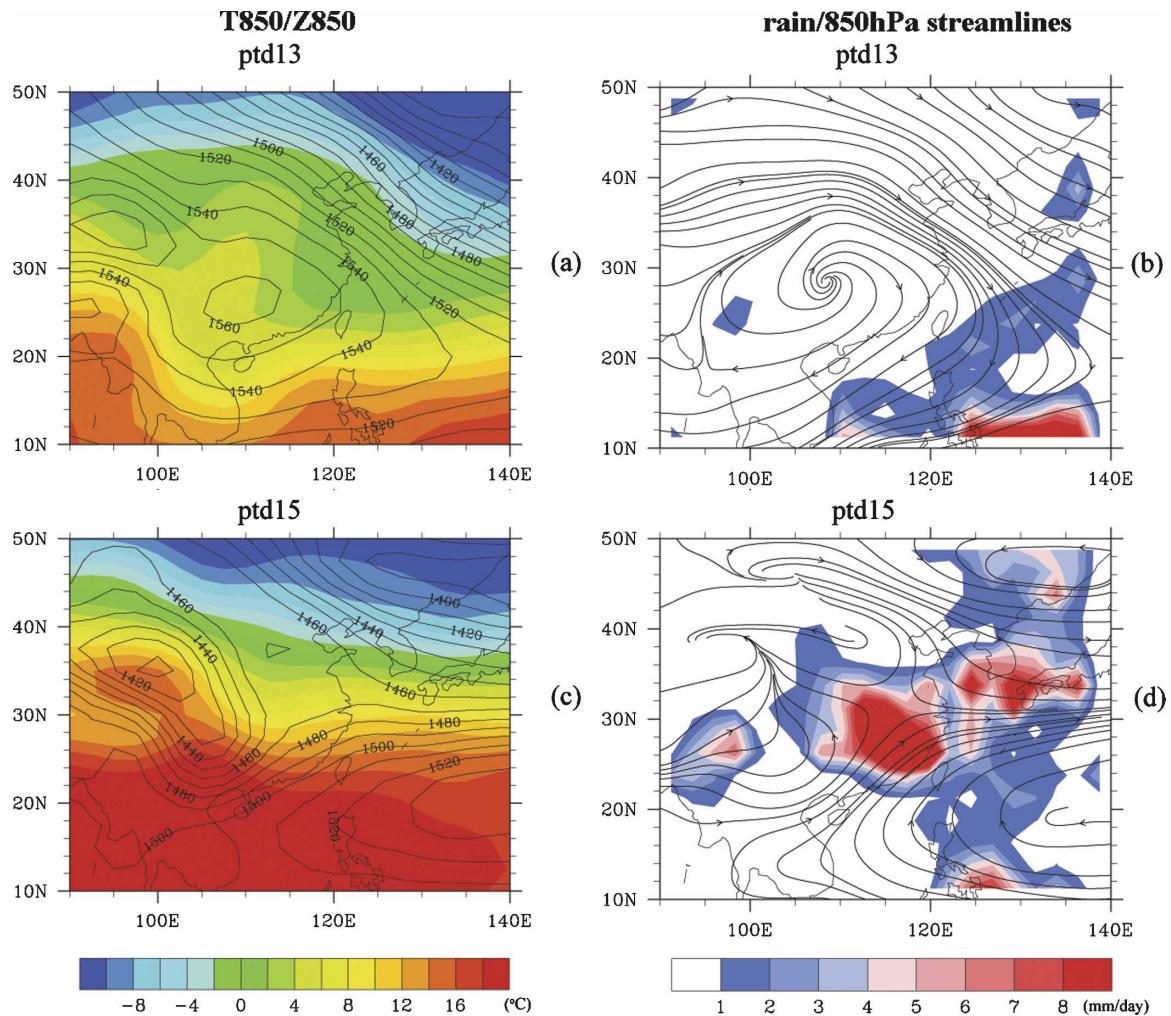
FIG. 5. (a) NCEP 850-hPa temperature field (color shading) and geopotential height field (black contour lines), and (b) GPCP precipitation (color shading) and NCEP 850-hPa streamlines, all for pentad 13 in 1986. (c), (d) As in (a), (b), but for pentad 15 in 1986.

which are located on the southern flank of the weakening westerly jet stream in the upper troposphere (Fig. 4b). This cyclonic tendency could modulate low-level synoptic development over those regions. The patterns in Figs. 5a,b show that, in pentad 13 (2–6 March), south China is still under the influence of a low-level anticyclone. These charts also indicate the prevalence of cold-air advection to central China and south China, and no significant precipitation in that region. A shallow trough is developing to the northwest of the anticyclone. In pentad 15 (12–16 March), deepening of this trough leads to the formation of an extensive cyclone system over western China. Abundant moisture is transported to south China by the enhanced low-level southwesterly flow (Fig. 5d). The strong temperature gradients at 850 hPa (Fig. 5c) and the associated precipitation (Fig. 5d) in pentad 15 are indicative of a favorable synoptic environment for frontal activities over

south China. These developments result in persistent and significant rainfall (>5 mm day^{-1}) over south China (Figs. 5d and 4a). This rainfall marks the onset of the SCSR. The SCSR lasts for about 2 months, and is followed by the onset of the South China Sea monsoon in mid-May (Wang et al. 2004). LinHo and Wang (2002) noted that, within the pre-mei-yu period from mid-May to June, continuous and heavy rainbands migrate from the tropics to subtropics (see also Fig. 4a), and the cross-equatorial divergent winds in the upper troposphere reverse direction (Fig. 4c).

b. Climatological averages

The case study of year 1986 in section 4a suggests that the SCSR onset is concomitant with the passage of the dry phase of a MJO in mid-March, which operates in concert with the slowly varying seasonal components, with accompanying attenuation of the local
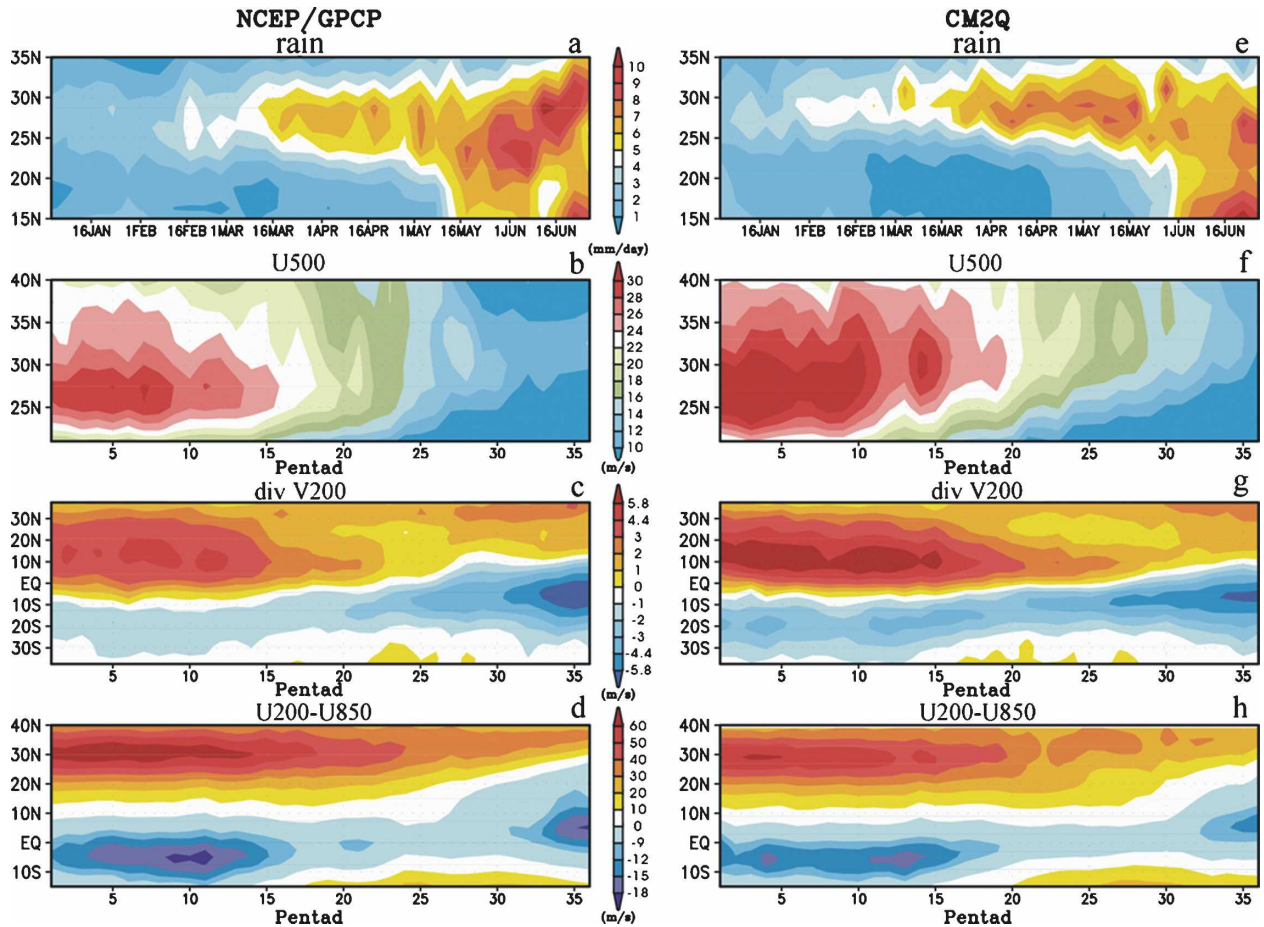
FIG. 6. Time–latitude distributions of observed climatological (a) rainfall rate, (b) 500-hPa zonal wind, (c) 200-hPa meridional divergent wind (m s^{-1}), and (d) difference between zonal wind at 200 and 850 hPa (m s^{-1}). (e)–(h) Model counterparts of (a)–(d) based on output from the CM2Q experiment for a 20-yr period. All results are obtained by averaging the data over 110°–130°E.

Hadley cell and the East Asian jet stream. The slow seasonal components participating in this evolution include changes of land–ocean thermal contrast in East Asia and the meridional thermal contrast due to the seasonal march of insolation. To delineate the role of these seasonal forcings in the circulation and precipitation changes described in section 4a, it is instructive to examine the seasonal variation of the climatological averages of various signals associated with SCSR. The counterpart of Fig. 4, as computed using observed and simulated climatological means instead of data for a single year, is displayed in Fig. 6. The 22-yr averages of NCEP and GPCP data (Figs. 6a–d) show an increase in baroclinity within the 0°–10°S zone, and corresponding changes in 200-hPa northward divergent wind and 500-hPa zonal winds near mid-February. Following this period of intensification is a decrease in 200-hPa meridional divergent wind, weakening of the East Asian jet stream, and emergence of SCSR in mid-March. A simi-

lar sequence of events is discernible from 20-yr averages of the model output (Figs. 6e–h). The climatological charts in Fig. 6 show a distinct period of intensification of the local Hadley cell, followed by a period of attenuation. The appearance of such rapid variations in long-term averaged patterns is suggestive of the contributions of higher-frequency phenomena with phases that are tied with the slow seasonal march. Candidates for such "phase-locked" phenomena include MJO in the tropics, and various circulation features in the midlatitudes.

5. Typical evolution of flow patterns prior to and after the SCSR onset

To delineate the key atmospheric variations during the transition from the winter to spring regimes, we proceed to document the salient circulation changes associated with the SCSR onset. Such analysis requires

the determination of onset dates for individual years. The onset date in a particular year can be identified by using data for that year to construct diagrams similar to those in Figs. 4 and 6. The following criteria are applied to the observational datasets, so as to obtain the SCSR onset dates in individual years of the 1979–2002 period:

1) Occurrence of the first persistent rain episode (at least two consecutive pentads with mean precipitation rate >6 mm day^{-1}) in the calendar year in south China (24°–32°N, 110°–130°E).
2) Deceleration and northward retreat of the boreal winter subtropical westerly jet at 500 hPa (<30 m s^{-1} over 25°–35°N, 110°–130°E).
3) Coherent weakening of northward divergent wind at 200 hPa (<4 m s^{-1} over 5°–25°N, 110°–130°E).
4) Termination of the Indonesian–Australian summer monsoon, as inferred from high outgoing longwave radiation (OLR) values (>230 W m^{-2}) over that region (15°S–0°, 110°–130°E).

The SCSR onset date in each year of the 1979–2002 period generally satisfies the four joint criteria listed above. In some years there is a premature rain spell that agrees with the first criterion, but is not accompanied by the changes as prescribed by the other criteria. In such years a subsequent surge of spring rain turns out to be more consistent with all four criteria, and the latter event is chosen to be the SCSR onset. The onset dates identified here will be used later to construct composite maps.

As for output from the CM2Q experiment, we obtain the SCSR onset dates and the composite maps using the following method. From the model output for a 100-yr period (model years 101–200), we select those years in which an onset pentad of the SCSR can be identified in an unambiguous manner. This identification procedure uses the same criteria as mentioned above, except that the numerical thresholds are adjusted to accommodate differences between the observed and model climatologies. We then generate composite maps based only on these model years with a well-defined onset date. In total, onset dates can be determined in 60 out of the 100 available model years.

The average onset pentad of the SCSR as obtained from observations in the 1979–2002 period is pentad 15 (12–16 March), with a standard deviation of 2.0 pentads. The average onset pentad based on model output is pentad 16 with a standard deviation of 2.6 pentads. In view of the considerable spread among the onset pentads in individual years, some of the rapid transitions accompanying SCSR onset might not be apparent in the climatological charts presented in the previous sec-

tions, due to smoothing of such features in the time-averaging process.

Figure 7 shows the composite evolution of the 20–80-day filtered 200-hPa velocity potential, within the time span from the fourth pentad before (hereafter, pentad −4) to the fourth pentad after (hereafter, pentad +4) the SCSR onset. The observed evolution (NCEP, left panels of Fig. 7) is based on composites over the entire 24-yr (1979–2002) period. The model patterns (CM2Q, right panels of Fig. 7) are based on composites over 60 selected years, as mentioned before. Note that the composite charts in Fig. 7 depict the typical evolution of the filtered velocity potential field relative to the SCSR onset, which falls on different dates in individual years. The statistical significance of the velocity potential anomalies is determined using the Student's t test, and is indicated in each panel of Fig. 7 by gray shading. A majority of the features noted in the following discussion surpass the 95% significance level.

The observational results (left panels of Fig. 7) indicate that there is typically a MJO event traveling around the globe during the nine-pentad period centered on the SCSR onset, thereby switching on and off various local convection centers. Before the SCSR onset, the wet phase of the MJO (negative velocity potential values) travels at a slow speed ($\sim 4.5°$ longitude per day at the equator) from the western Pacific to the central Pacific. From pentad −1 to the onset pentad, the wet phase quickly passes through the eastern Pacific and reaches tropical Africa. At the same time, the dry phase (positive values) occupies a vast region extending from the eastern Indian Ocean to the central Pacific. The center of the dry phase at the onset pentad is situated over the Philippines, Indonesia, and northern Australia. The arrival of this signal is coincident with the decline of the Indonesian–Australian summer monsoon.

As shown in the right panels of Fig. 7, the model also simulates a MJO traveling around the globe before and after the SCSR onset. As in the observational composite maps, the center of the dry phase of this model-generated MJO is also located over the Maritime Continent and northern Australia at the onset pentad. Hence, both model and observational results indicate that intraseasonal convective activity could contribute to the near-equatorial and extratropical circulation changes during the SCSR onset. The overall consistency between the climatological findings in section 4b and the composite charts in Fig. 7 also confirms the appropriateness of the criteria for identifying the onset pentads, on which the composite procedure is based. The amplitude of the simulated MJO, as represented by the velocity potential variations, is considerably weaker
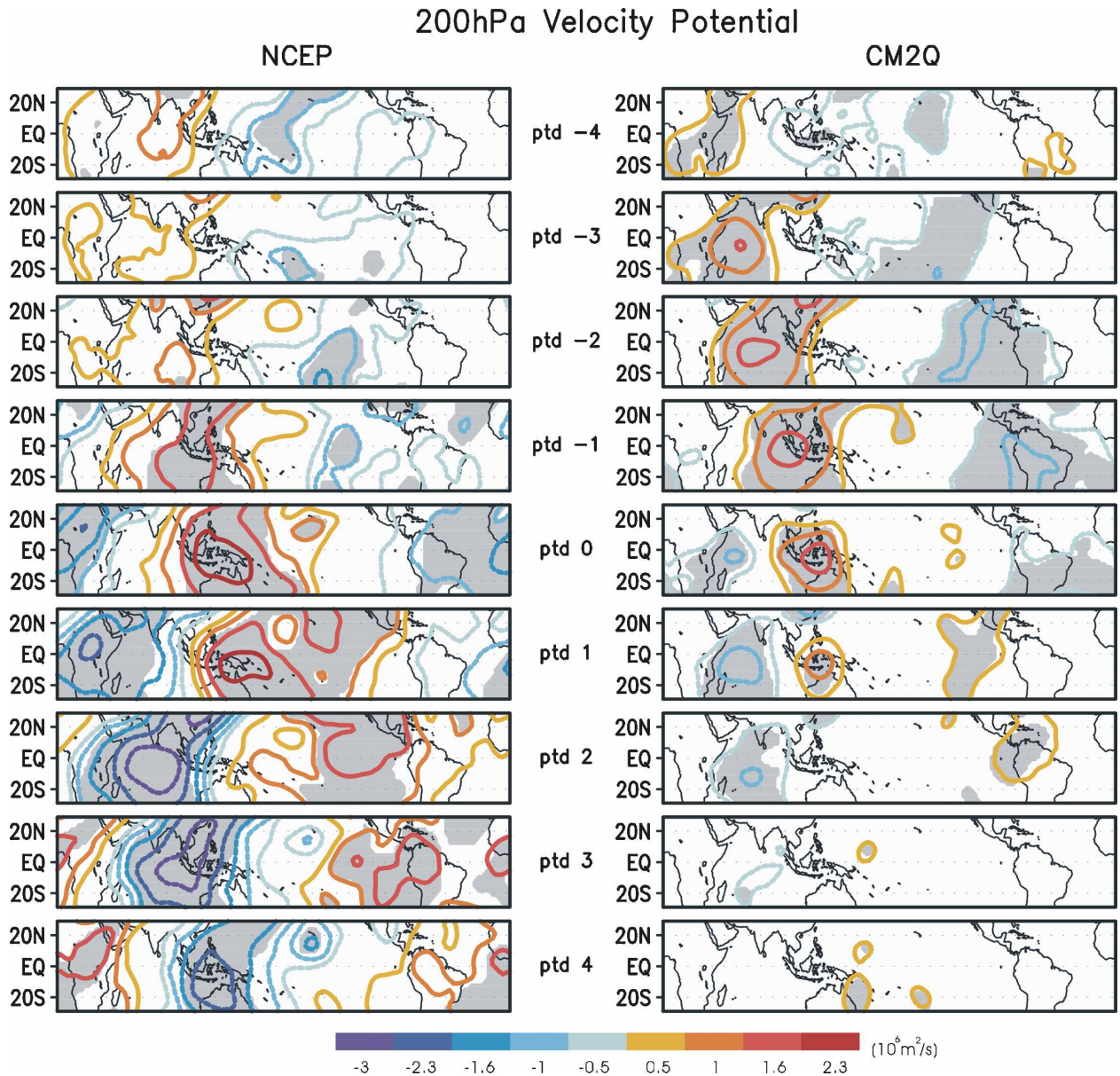
200hPa Velocity Potential

FIG. 7. (left) Evolution of composite maps of 20–80-day bandpass-filtered NCEP 200-hPa velocity potential (10^6 m^2 s^{-1}) from lag -4 to lag $+4$ with respect to the SCSR onset pentad, as obtained by using data for the entire 1979–2002 period. (right) Model counterparts from the CM2Q experiment, as obtained using data for 60 selected yr out of the total sample of 100 yr (refer to section 5 for more details of the selection). Gray shading indicates values exceeding 95% significance as determined by Student's t test.

than that observed in both the dry and wet phases. From pentad -3 to the onset pentad, the simulated speed of the wet phase propagation is notably different from its observed counterpart. This discrepancy is suggestive of insufficient representation of the interaction between convection and large-scale dynamics in the model tropics.

To describe the evolution of the tropical divergent circulation on time scales of a season and longer, the sum of the second to fourth annual harmonics (which

retain periods between 90 and 180 days) of the area-averaged 200-hPa velocity potential field in the 20°S–20°N zone is computed. The composite of this quantity relative to the SCSR onset pentad is displayed in Fig. 8 as a function of longitude (abscissa) and time lag (ordinate), for NCEP (left panel) and CM2Q (right panel) data. The NCEP composite shows that, over the Maritime Continent and western Pacific, this slow-varying seasonal component is characterized by a transition from a wet phase near pentad -6 to a dry phase near
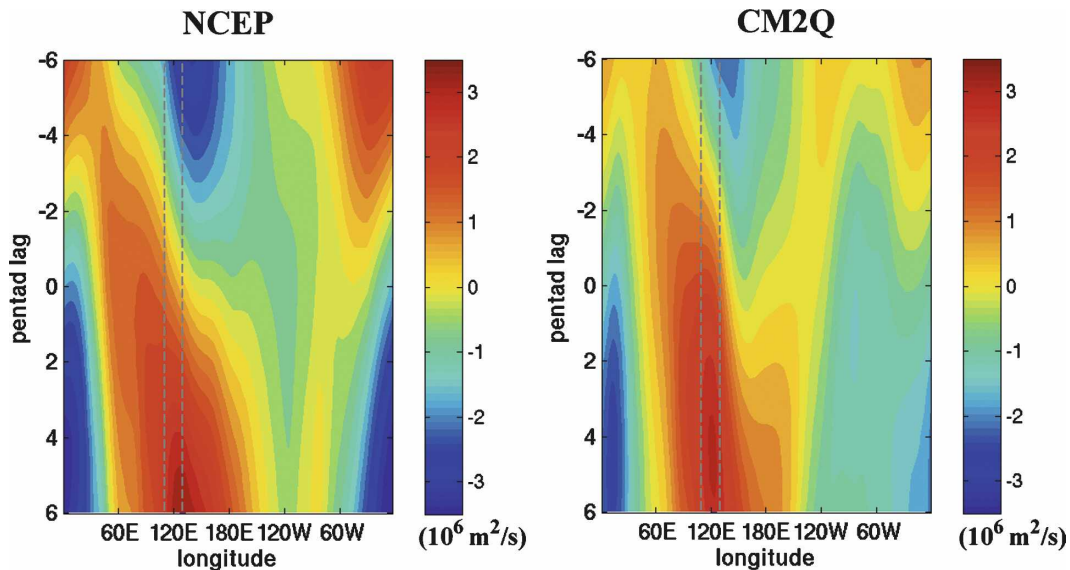
FIG. 8. Longitude–time distributions of the composite of the sum of the second–fourth annual harmonics of 200-hPa velocity potential (10^6 m^{2}s^{-1}) averaged over 20°S–20°N. Time lags on the ordinate axis are defined relative to the SCSR onset pentad. (left) Based on NCEP data for the entire 1979–2002 period. (right) Based on 60 selected yr out of 100 yr in the CM2Q experiment. The East Asia sector (110°–130°E) is marked with gray dashed lines.

pentad +6. The sign reversal of this low-frequency signal occurs near pentad −2, and is coincident with the rapid termination of the wet phase of the MJO over the same region (see Fig. 7). Opposite changes in the low-frequency component are evident in the Atlantic sector (40°W–20°E), with a dry phase before the SCSR onset evolving to a wet phase thereafter. These developments in the observed annual harmonics during the SCSR onset are reproduced by the GCM to a large degree (right panel of Fig. 8). The results in Fig. 8, as constructed on the basis of *composites* of low-frequency fluctuations in each individual years relative to the SCSR onset, are almost identical to the corresponding plots for time–longitude development of *climatologically averaged* data for consecutive pentads (i.e., pentads 9–21) of the calendar year (not shown here).

Within the 110°–130°E sector, the coincidence of the wet-to-dry transitions associated with both the 20–80- and 90–180-day frequency bands is indicative of substantial temporal correspondence between intraseasonal (MJO) activities and slower seasonal migrations during the onset stage of SCSR. This relationship is similar to that between the fast annual cycle and slow annual cycle associated with the Asian summer monsoon (LinHo and Wang 2002). As described in sections 3 and 4, the passage of the dry phase of a MJO reinforces the slow seasonal evolution of the atmospheric circulation. The weakening of the thermally direct cell contributes to the termination of the winter circulation

regime over the East Asian sector and the establishment of the spring regime that lasts until mid-May. This transition occurs within a relatively short period (~2 pentads). Such distinctive transition in East Asia during spring, of which the SCSR onset is a prime example, may partially be attributed to the joint effects of MJO variability and the seasonal march.

The SCSR onset is accompanied by a series of adjustments in both the tropics and higher latitudes. To delineate these changes, we subtract the composite of selected variables over the pentads −1 and −2 from the corresponding composite over the pentads +1 and +2. These differences in the observed streamline pattern and geopotential height at 200 and 850 hPa are shown in Figs. 9a and 9b, respectively. The attenuation of the principal wintertime upper-level troughs and ridges can be clearly seen from Fig. 9a. For example, the strength of upper-level troughs over the western North Pacific (T1) and North Atlantic (T2) is reduced. Similarly, the ridges over Siberia (R1), Azores (R2), and Alaska (R3) are weakened. A zone of easterly wind differences prevails at about 30°N near the date line. This feature is indicative of the drastic weakening of the local westerly jet stream during the SCSR onset. To the north of this zone, there is anticyclonic tendency at both 200 (Fig. 9a) and 850 hPa (Fig. 9b). To the south of this zone, a cyclonic tendency can be well identified at the 200-hPa level, but not at the 850-hPa level. The prominent anticyclonic center at 850 hPa over the northwestern Pa-
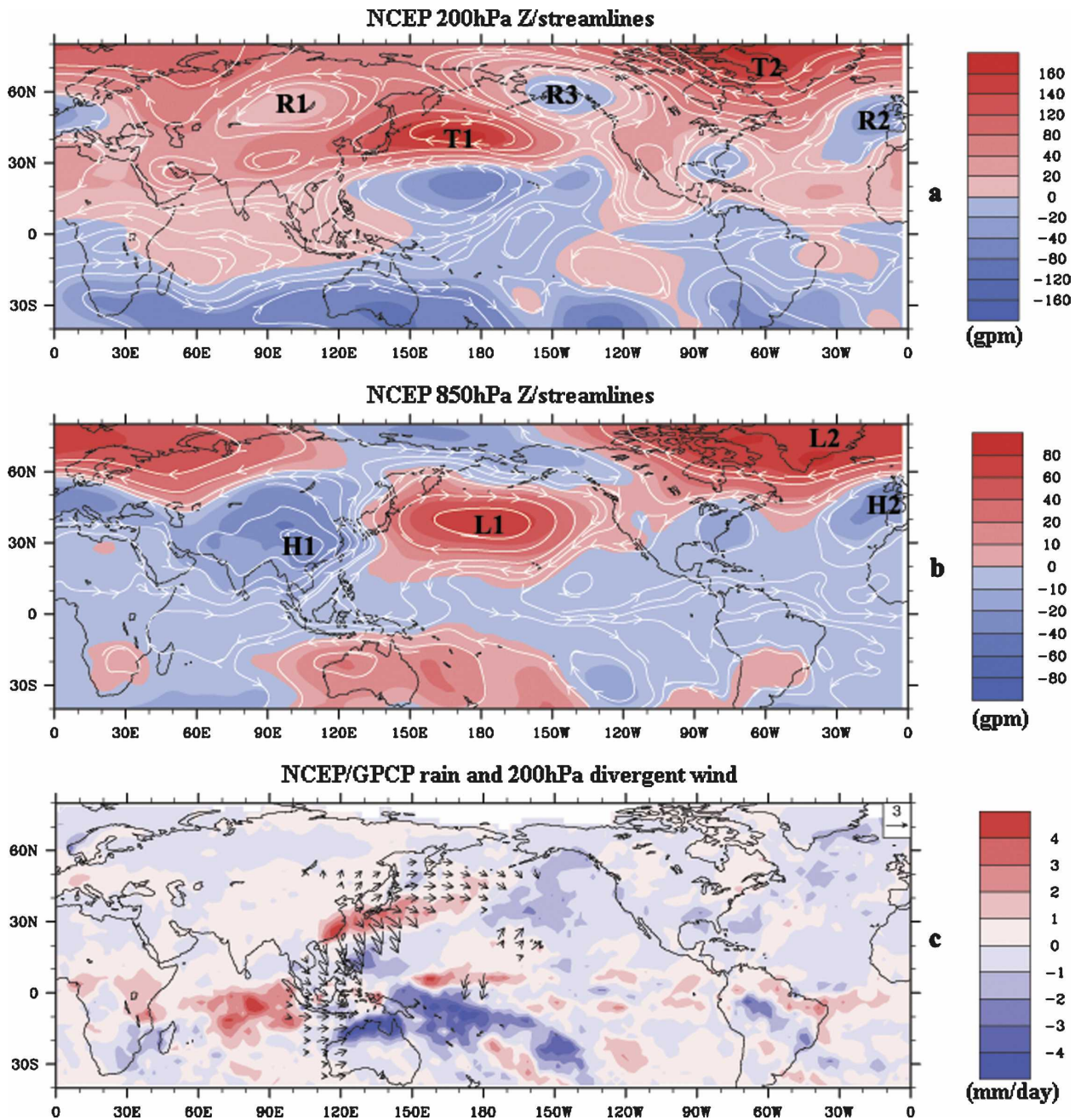
FIG. 9. (a) Difference charts as obtained by subtracting the composite NCEP 200-hPa height and streamline pattern in pentads −1 and −2 (before SCSR onset) from the corresponding composites in pentads +1 and +2 (after onset). Principal ridges and troughs are labeled using prefixes "R" and "T," respectively. (b) As in (a), but for 850-hPa height and streamlines. Major highs and lows are marked using prefixes "H" and "L," respectively. Note that the charts depict the weakening of the major ridges/troughs or highs/lows in the course of SCSR onset, not the ridges/troughs or highs/lows themselves. (c) As in (a), but for GPCP precipitation (mm day^{-1}; color shading) and NCEP 200-hPa divergent wind with difference exceeding 1 m s^{-1} (arrows). All observational results are based on data for the entire 1979–2002 period. (d)–(f) Model counterparts of (a)–(c), as computed using output for 60 selected yr out of 100 yr in the CM2Q experiment.

cific, together with the cyclonic tendencies over sub-tropical southeastern Asia (Fig. 9b), are indicative of the influences of the weakening wintertime land–sea thermal contrast on the low-level circulation pattern. In

Fig. 9b, a low-level confluence zone with increased northeastward flow is seen to extend from Southeast Asia to the Korean Peninsula. This zone is almost collocated with the south China spring rain belt as shown
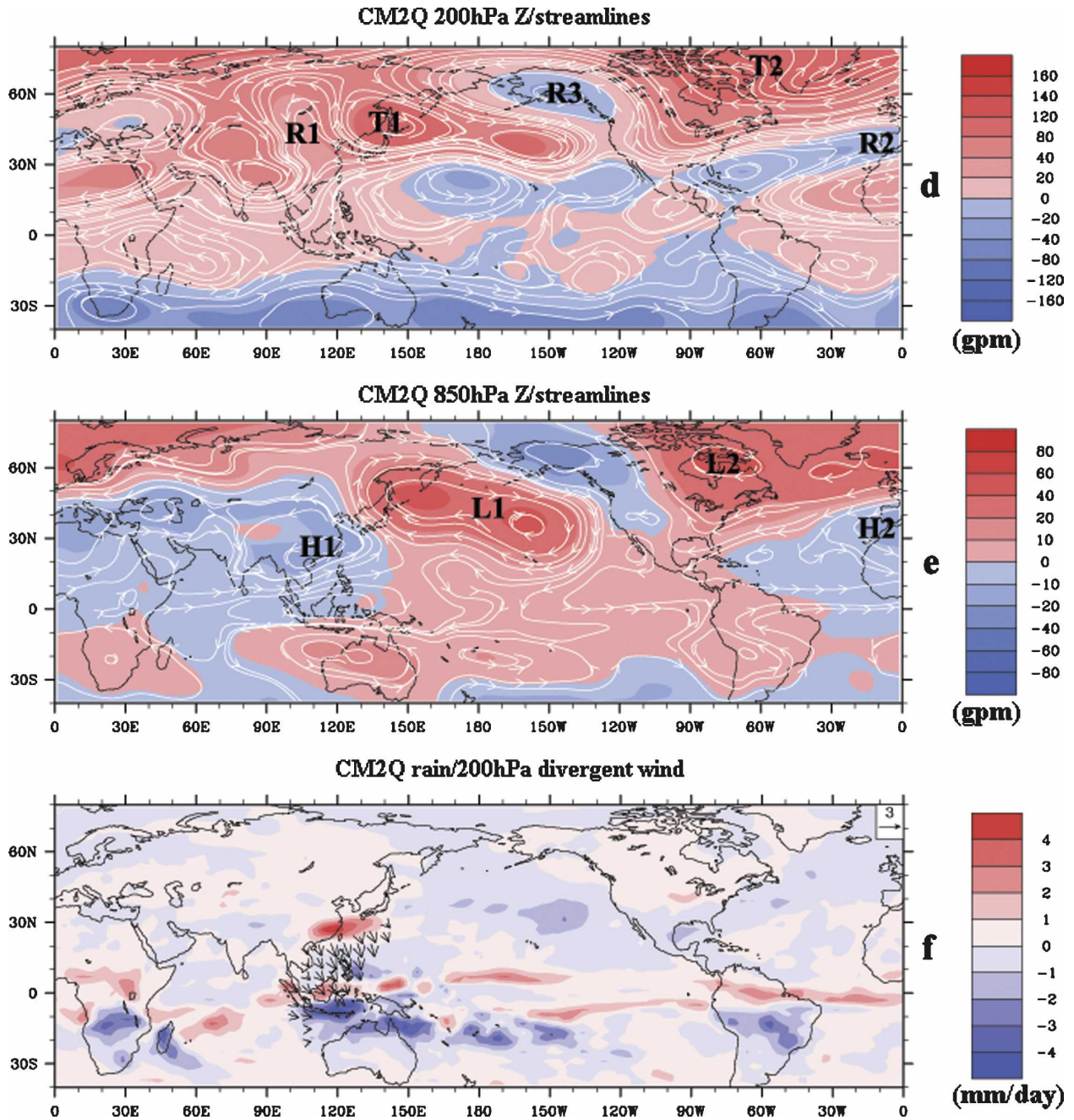
FIG. 9. (*Continued*)

in Fig. 3. The reduced intensities of the Siberian high (H1), Aleutian low (L1), Azores high (H2), and Iceland low (L2) are also evident in Fig. 9b. In Figs. 9a,b, the patterns in the Indian Ocean sector are indicative of paired centers of low-level cyclonic tendencies and upper-level anticyclonic tendencies straddling the equator. These features may be forced by the enhanced convection over the eastern Indian Ocean (see Fig. 9c). Analogously, paired centers of anticyclonic tendencies

at 850 hPa and cyclonic tendencies at 200 hPa prevail in the western Pacific–Australian sector. This pattern could be the response to suppressed convection over the western Pacific.

Figure 9c shows the corresponding changes in GPCP rainfall and NCEP 200-hPa divergent wind in the course of the SCSR onset. The much reduced convective activity over Indonesia–Australia and the SPCZ is indicated by convergence of upper-level divergent

winds and large negative precipitation differences over that area. Meanwhile, large precipitation increases and strong divergence of upper-level winds prevail in the SCSR region along the East Asian coast. The strong divergent winds in this sector could be associated with both reduced tropical convection and increased local precipitation. Over the western Pacific east of the Philippines, there is another center of negative precipitation differences. This feature, together with positive center associated with the south China rain belt farther north, are indicative of a fast poleward shift of rainfall over that region. In the midlatitude zone, the precipitation decrease and enhanced upper-level convergence in the eastern portion of the Pacific storm track during the SCSR onset are apparent in Fig. 9c.

The corresponding difference charts based on CM2Q output are presented in Figs. 9d–f. The upper-level planetary wave adjustments in the mid- and high latitudes are well captured in the model (Fig. 9d). The difference chart at 850 hPa (Fig. 9e) is generally consistent with the observed pattern (Fig. 9b), though the aforementioned paired centers of low-level cyclonic tendency in the Indian Ocean sector is less apparent in the simulated pattern. The simulated precipitation differences over the SPCZ (Fig. 9f) are noticeably weaker than observed. The northeastward extent of the simulated positive precipitation differences over south China is less than that in the observed pattern. This discrepancy is consistent with the precipitation charts presented in Fig. 3. The simulated differences in the 200-hPa divergent wind are generally weaker than observed, especially on the northern and eastern flanks of the SCSR. Generally speaking, the model is capable of reproducing the global adjustments to the shutdown of the Indonesian–Australian summer monsoon.

6. Conclusions and discussion

The SCSR onset is a distinct signal associated with the transition of the global atmospheric circulation from boreal winter to spring. The increase of insolation over the Northern Hemisphere from January to March gradually weakens the thermal contrast between the continent and ocean, as well as the general north–south surface temperature gradient. In conjunction with these slow processes, a passage of the dry phase of a MJO over the Indonesian Maritime Continent around mid-March is coincident with the termination of the Indonesian–Australian summer monsoon and reduction in convective activities in that region. This combination of events leads to a rapid weakening of the local interhemispheric Hadley cell, which is in turn followed by deceleration of the upper-level jet stream over East

Asia, the onset of the SCSR, and the rapid westward expansion of the subtropical Pacific high. This family of phenomena signifies a structural change of the atmospheric circulation in the Asian–Pacific sector from boreal winter to spring. Concurrent midlatitude local processes in the East Asian sector could also influence the aforementioned structural changes, including the SCSR onset.

Diagnosis of the physical causes of the changes associated with SCSR onset is an important step toward a more complete understanding of the cross-season memory of the Asian monsoon from winter to summer. On the basis of the findings presented in the previous sections, these physical mechanisms may be summarized as follows. In mid-March, the passage of the dry phase of a MJO over the Indonesian–Australian sector is accompanied by reduced convection in that area. This event operates in concert with seasonal changes of thermal contrast, and contributes to attenuation of the interhemispheric local Hadley cell in this sector. The reduced convective heating in the deep tropics forces a teleconnection pattern over the central and western North Pacific that has been well studied by other investigators (e.g., Ferranti et al. 1990; Schubert and Park 1991; Matthews et al. 2004). The suppressed tropical convection is associated with jet deceleration and other midlatitude circulation changes. We again note that various midlatitude processes (e.g., seasonal shifts in planetary wave structure, storm-track activities, etc.) could also contribute to jet deceleration. In the region located north of the wintertime jet stream, the change is characterized by an anomalous anticyclone (see circulation in the vicinity of T1 in Figs. 9a and 9d). This feature is associated with weakening of the East Asian jet stream at 30°N, and the strengthening of the zonal wind at ~55°N (i.e., a northward shift of the jet axis). In the region south of the wintertime jet stream, cyclonic tendency prevails in the upper troposphere. This feature extends toward south China and the adjacent oceanic areas, and could favor the development of low-level troughs over that location. It is noteworthy that the weakening land–sea thermal contrast also contributes to the development of low-level troughs over this region. Intensification of the low-level southwesterly flow over the East Asian seaboard leads into increased moisture transport from the tropics to south China. Together with the low-level cyclonic tendencies, this synoptic environment favors frontal development and precipitation over south China. The weakening of the jet stream intensity (Fig. 4) leads to reduced eastward steering of the transient disturbances by the mean circulation. The rapid westward expansion of the Pacific subtropical high (Fig. 3) serves to block the eastward

migration of frontal systems originating from East Asia. Both effects contribute to stagnation of weather systems over south China, thus resulting in more frequent occurrence of stationary frontal zones over that region.

Newman and Sardeshmukh (1998) used a linear barotropic model to demonstrate that the midlatitude response to the MJO divergent forcing is highly sensitive to the change of seasonal base state, especially in early spring. Their results suggest that in early spring (March) the large-scale background flows facilitate optimal forcing of the midlatitude circulation by tropical convection. This inference supports our findings concerning the role of MJO in the winter-to-spring transition in East Asia.

Besides the above physical connection between tropical activities and the SCSR onset, extratropical processes can have considerable influences on the jet stream and the precipitation process in south China during the winter-to-spring transition. For instance, the revival of the Pacific storm-track activity after its midwinter suppression (Nakamura 1992) could modulate the precipitation over south China. Given that the present investigation is primarily concerned with the relationship between tropical activities and SCSR onset, the detailed documentation of the extratropical influence or evaluation of the relative importance of tropical and extratropical influences are beyond the scope of this study. Yet these topics are worthy of further investigation and would enhance our understanding of the SCSR. For most parts of East Asia and the western Pacific, the SCSR onset may be viewed as the start of boreal spring; whereas the South China Sea onset in May–June (see Fig. 1) may be deemed as the end of this season. A prominent feature of boreal spring is the zonal elongation of the subtropical Pacific high (Fig. 3), with its western edge almost connecting with the circum-global ridge line at ~30°N. This distinct zonal symmetry suggests that the planetary-scale circulation accommodates more to the astronomical solar forcing in boreal spring than in any other season. The tropical flow patterns in other seasons are more prone to local monsoon influences, which lead to strong zonal asymmetries. As noted by Hung et al. (2004) and many others, because of their considerable thermodynamic inertia, the monsoon systems (especially the Asian summer monsoon) possess prolonged, cross-seasonal memory. Hence, the relatively weak monsoon influences in boreal spring offer a window of opportunity for the climate system in the Asian and Australian sector to reset itself as each new Asian monsoon year (May–April) begins (Yasunari 1991). This notion is in accord with the numerical experiments carried out by Webster

(1995), which indicate drastic reduction of predictability across the boreal "spring barrier."

The CM2Q experiment, to a large extent, captures the essential features of the seasonal transition in the boreal spring. The simulated climatological evolution in the East Asian sector during this winter-to-spring transition, as illustrated in Figs. 3 and 6, is quantitatively consistent with observed climatology. The most notable discrepancy between the model and observation is related to the characteristics of intraseasonal variability (see Fig. 7). This disparity between model and observation has also been reported by the GFDL Global Atmospheric Model Development Team (2004), who showed that the MJO activity in the model atmosphere is generally weaker and less coherent than that inferred from observations. The SCSR onset is simulated rather well by the model in spite of its underestimation of the MJO amplitude. These model results suggest that the SCSR onset does not depend on the strength of MJO activity alone, and that the possible contributions of midlatitude processes to the SCSR onset should also be considered. The considerable agreements between the simulated and observed atmospheres in other aspects of the SCSR phenomenon offer impetus to utilize this GCM for studying various issues related to monsoon climate (e.g., interdecadal variability of this SCSR event and the contributions of different factors to such fluctuations). Carefully designed model experiments are helpful for gaining insights to low-frequency variability by virtue of the large sample sizes obtainable from multicentury integrations, and utility of the simulations for testing physical hypotheses. After demonstrating the model's capability to reproduce the essential features in the observed atmosphere, we could apply with some confidence this model tool to enhance our understanding of the climatological and time-varying aspects of monsoon climate.

REFERENCES

Blackmon, M. L., J. M. Wallace, N.-C. Lau, and S. M. Mullen, 1977: An observational study of the Northern Hemisphere wintertime circulation. *J. Atmos. Sci.,* **34,** 1040–1053.

Cheang, B.-K., 1986: Short- and long-range monsoon prediction in

Southeast Asia. *Monsoons,* J. S. Fein and P. L. Stephens, Eds., John Wiley, 579–606.

Chen, G. T.-J., Z. Jiang, and M.-C. Wu, 2003: Spring heavy rain events in Taiwan during warm episodes and the associated large-scale conditions. *Mon. Wea. Rev.,* **131,** 1173–1188.

Delworth, T. L., and Coauthors, 2006: GFDL's CM2 global coupled climate models. Part I: Formulation and simulation characteristics. *J. Climate,* **19,** 643–674.

Ding, Y., 2004: Seasonal march of the East Asian summer monsoon. *East Asian Monsoon,* C.-P. Chang, Ed., World Scientific, 3–53.

Ferranti, L., T. N. Palmer, F. Molteni, and E. Klinker, 1990: Tropical–extratropical interaction associated with the 30–60 day oscillation and its impact on medium and extended range prediction. *J. Atmos. Sci.,* **47,** 2177–2199.

GFDL Global Atmospheric Model Development Team, 2004: The new GFDL global atmosphere and land model AM2–LM2: Evaluation with prescribed SST simulations. *J. Climate,* **17,** 4641–4673.

Hsu, H.-H., B. J. Hoskins, and F.-F. Jin, 1990: The 1985/86 intraseasonal oscillation and the role of the extratropics. *J. Atmos. Sci.,* **47,** 823–839.

Hung, C., X. Liu, and M. Yanai, 2004: Symmetry and asymmetry of the Asian and Australian summer monsoons. *J. Climate,* **17,** 2413–2426.

Kalnay, E., and Coauthors, 1996: The NCEP/NCAR 40-Year Reanalysis Project. *Bull. Amer. Meteor. Soc.,* **77,** 437–471.

Lau, K.-M., and M.-T. Li, 1984: The monsoon of East Asia and its global associations—A survey. *Bull. Amer. Meteor. Soc.,* **65,** 114–123.

LinHo, and B. Wang, 2002: The time–space structure of the Asian–Pacific monsoon: A fast annual cycle view. *J. Climate,* **15,** 2001–2019.

Madden, R. A., and P. R. Julian, 1971: Detection of a 40–50 day oscillation in the zonal wind in the tropical Pacific. *J. Atmos. Sci.,* **28,** 702–708.

Matthews, A. J., B. J. Hoskins, and M. Masutani, 2004: The global response to tropical heating in the Madden–Julian oscillation during northern winter. *Quart. J. Roy. Meteor. Soc.,* **130,** 1991–2012.

Nakamura, H., 1992: Midwinter suppression of baroclinic wave activity in the Pacific. *J. Atmos. Sci.,* **49,** 1629–1642.

Newman, M., and P. D. Sardeshmukh, 1998: The impact of the annual cycle on the North Pacific/North American response to remote low-frequency forcing. *J. Atmos. Sci.,* **55,** 1336–1353.

Schubert, S. D., and C. K. Park, 1991: Low-frequency intraseasonal tropical–extratropical interactions. *J. Atmos. Sci.,* **48,** 629–650.

Tian, S. F., and T. Yasunari, 1998: Climatological aspects and mechanism of spring persistent rains over central China. *J. Meteor. Soc. Japan,* **76,** 57–71.

Ueda, H., T. Yasunari, and R. Kawamura, 1995: Abrupt seasonal change of large-scale convection activity over the western Pacific in northern summer. *J. Meteor. Soc. Japan,* **73,** 795–809.

Wan, R. J., and G. X. Wu, 2007: Mechanism of the spring persistent rains over southeastern China. *Sci. China Ser. D: Earth Sci.,* **50,** 130–144.

Wang, B., LinHo, Y. Zhang, and M.-M. Lu, 2004: Definition of South China Sea monsoon onset and commencement of the East Asia summer monsoon. *J. Climate,* **17,** 699–710.

Webster, P. J., 1995: The annual cycle and the predictability of the tropical coupled ocean-atmosphere system. *Meteor. Atmos. Phys.,* **56,** 33–55.

Wu, R., and B. Wang, 2001: Multi-stage onset of summer monsoon over western North Pacific. *Climate Dyn.,* **17,** 277–289.

Xie, P., J. E. Janowiak, P. A. Arkin, R. Adler, A. Gruber, R. Ferraro, G. J. Huffman, and S. Curtis, 2003: GPCP pentad precipitation analyses: An experimental dataset based on gauge observations and satellite estimates. *J. Climate,* **16,** 2197–2214.

Yasunari, T., 1991: The monsoon year—A new concept of the climate year in the tropics. *Bull. Amer. Meteor. Soc.,* **72,** 1331–1338.

Zhu, Q. G., J. R. Lin, and S. W. Shou, 1981: *Principles and Methods in Synoptic Meteorology* (in Chinese). Beijing Meteorological Press, 535 pp.